THE JOURNAL OF PHYSICAL CHEMISTRY A
A JOURNAL OF THE AMERICAN CHEMICAL SOCIETY

pubs.acs.org/JPCA

Article

Femtosecond Wavepacket Dynamics Reveals the Molecular Structures in the Excited (S_1) and Cationic (D_0) States

Junggil Kim,[†] Kyung Chul Woo,[†] and Sang Kyu Kim*

Cite This: https://doi.org/10.1021/acs.jpca.1c04976

Read Online

ACCESS | Metrics & More | Article Recommendations | Supporting Information

ABSTRACT: Molecular structures in the electronically excited (S_1) and cationic (D_0) states of 2-fluorothioanisole (2-FTA) have been precisely refined from the real-time dynamics of the femtosecond (fs) wavepacket prepared by the coherent excitation of the Franck−Condon active out-of-plane torsional modes in the $S_1 \leftarrow S_0$ transition at 285 nm. The simulation to reproduce the experiment in terms of the beating frequencies gives the nonplanar geometry of 2-FTA in S_1, where the out-of-plane dihedral angle (φ) of the S-CH_3 moiety is 51° with respect to the molecular plane. The behavior of the fs wavepacket in terms of the amplitudes and phases with the change of the probe (ionization) wavelength (λ_{probe} = 300−330 nm) provides the otherwise veiled structure of the cationic D_0 state. While the 2-FTA cation adopts the planar geometry (φ = 0°) at the global minimum, it is found to have a vertical minimum at $\varphi \approx 135°$ from the perspective of the $D_0 \leftarrow S_1$ vertical transition. *Ab initio* calculations support the experiment quite well although the simulation using the model potentials could improve the match with the experiment, giving the new interpretation for the previously disputed photoelectron spectroscopic results.

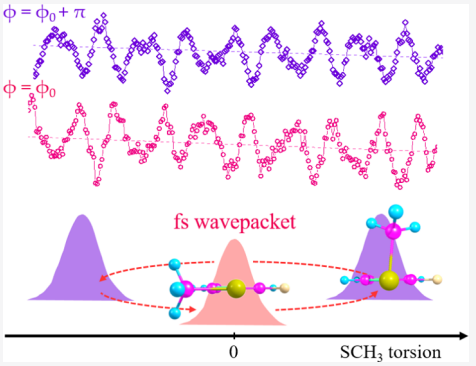

INTRODUCTION

Molecular structures dictate the fate of the chemical reactions. The conformational isomer, which could be converted to the other conformer quite easily by the nearly free internal rotation about the single bond axis, has been found to give a profound influence on the chemical reactivity.[1,2] In ambient conditions though, it would be nontrivial to confine the molecule to a specific geometry as all possible structural isomers may interconvert freely with very low barriers among them. In this respect, the spectroscopy and dynamics on the supersonically cooled molecular beam have been extremely useful as the internal energy is minimized so that the molecule is frozen at the minimum-energy geometry with respect to all normal mode coordinates in the ideal case where the vibrational temperature is also extremely low. Once the molecule is frozen at the specific geometry, it could be further utilized for chemical reactions such as the photodissociation/unimolecular reaction or stereospecific bimolecular reactions. When two or more structural isomers are populated together in the molecular beam, one can select just one specific isomer at a time by either the spectroscopic[3,4] or Stark deflection technique.[5−7] As a matter of fact, although rare, there are notable examples that report extremely interesting conformational specificity in chemical reactions.[8−10] In the photodissociation reactions, as the optical excitation is prompt, the phase space of the excited state is limited by the Franck−Condon window. If the excited state is repulsive along the particular bond extension coordinate, the initially chosen molecular geometry is then exactly reflected in the dynamic outputs. Namely, different geometrical isomer selection could lead to quite different outputs in terms of the rate, yield, and energy disposal dynamics, depending on the nature of the multidimensional excited-state potential energy surfaces.[8,9] The more elaborate case however could be found when the excited state is bound or quasi-bound. In this case, as long as the Franck−Condon overlap is nonzero, one can explore many different excited-state nuclear configurations spanned by individual vibronic modes. Especially when the internal energy of the excited state is small (e.g., <1000 cm^{-1}), the rate of intramolecular vibrational redistribution (IVR) is often slower than the rate of the excited-state reaction, giving the great opportunity to explore many different nuclear configurations of the excited state in terms of their chemical reactivities although the non-Franck−Condon region would be still blind.

The mode-selective reaction dynamics have long been investigated for many interesting chemical systems, which involve predissociation or tunneling process. The mode dependence of the dynamic outputs such as reaction rates and/or product yields has been extremely useful in disentangling the complicated coupling dynamics among

Received: June 6, 2021
Revised: July 13, 2021

numerous vibronic modes associated with the reaction channels. In this aspect, the dynamics around conical intersections have been studied in impressive detail in recent studies on thioanisoles,[11−17] thiophenols,[18−25] or phenols.[26−37] For instance, the nonadiabatic transition probability has been found to be strongly mode-dependent in the S-CH_3 bond predissociation of the electronically excited (S_1) thioanisole.[11,13,14,16,17] The nonadiabatic transition probability is strongly enhanced when (the nuclear configuration of the reactive flux given by) the specific vibronic mode accesses the conical intersection region. From the exploration of the wide range of the phase space, the otherwise formidable task of capturing the conical intersection in terms of the structure and its dynamic role becomes a reality now. The vibronic mode dependence has also been observed in the tunneling reactions. Namely, the tunneling in the H-atom detachment reactions of phenols and thiophenols turns out to be mediated by the upper-lying surface crossings in the proximity of the conical intersections along the multidimensional seam coordinates.[36−39]

As the direct optical transition has the intrinsic limit in terms of the Franck−Condon window, however, the expansion of the exploring region of the excited-state phase space is quite desirable for the investigation of multiple facets of the conical intersection, for example. One may employ the double resonance excitation technique such as the IR + UV scheme.[40,41] Here, the IR laser pulse prepares the specific rovibrational mode in S_0, whereas the subsequent UV excitation would then modify the accessible Franck−Condon region. Depending on the extent of IVR in S_0 prior to the UV excitation, the characteristic of accessible quantum states could also be modified. Interestingly, the other way to expand the exploring region of the excited state is the chemical substitution. A recent study of the photodissociation dynamics of 2-fluorothioanisole (2-FTA) is quite notable as it has been found that, unlike the case of thioanisole, it undergoes the substantial structural change upon the $S_1 \leftarrow S_0$ optical transition.[42] Namely, whereas thioanisole maintains its molecular planarity in the $S_1 \leftarrow S_0$ optical transition,[11,12,15] the planar 2-FTA in the ground state (S_0) undergoes the significant structural change to adopt the nonplanar geometry in S_1 in terms of the dihedral angle (φ) of the S-CH_3 moiety with respect to the molecular plane. As the S-CH_3 dihedral angle is one the most strongly coupled coordinates in the branching plane of the conical intersection,[12,13] the nonplanarity of the S_1 state should open the chance of exploring the S_1/S_2 conical intersection region from the completely different perspective; the otherwise veiled nonadiabatic path via the pseudo-conical intersection seam could be opened.[42] This approach is similar to the exploration of the other side of the moon. Even though the structural change upon the $S_1 \leftarrow S_0$ optical transition could be inferred from the spectroscopic evidence, it is not straightforward to grasp the exact shape of the excited-state potential energy surface, especially because the *ab initio* calculation of the excited state is quite challenging for polyatomic molecules at the present time.

Herein, we have found that the femtosecond coherent wavepacket interferometry is extremely useful in characterizing the excited-state geometry of 2-FTA. The molecular geometries of thioanisole and its derivatives have long been controversial in terms of the dihedral angle of the S-CH_3 moiety with respect to the molecular plane.[43−66] Although the presence of the geometrical isomer of $\varphi = 90°$ has been conjectured in many previous studies, thioanisole prepared in the supersonic jet has been found to adopt the planar geometry ($\varphi = 0°$) in the ground state as the global minimum structure.[57,65,66] As mentioned above, although thioanisole remains planar in S_1, 2-FTA becomes nonplanar upon the $S_1 \leftarrow S_0$ transition. The planar-to-nonplanar structural change of 2-FTA then allows the coherent excitation of the dihedral torsional modes within the coherence width of the femtosecond (fs) pump laser pulse.[67−74] The consequent fs wavepacket in S_1 propagates along the dihedral torsional angle (φ) coordinate, giving the clear-cut quantum beats in the parent ion transient obtained by monitoring the ionization cross section as a function of the delay time between the pump ($S_1 \leftarrow S_0$) and probe ($D_0 \leftarrow S_1$) fs laser pulses. Through the simulation of the experiment, the exact shape of the S_1 potential energy surface along the dihedral angle could be extracted. The D_0 structure could also be inferred from the apparent phase inversion of the quantum beat as the ionization wavelength is varied. The current fs wavepacket interferometry of 2-FTA unravels the detailed molecular structure of the S_1 state to give the most critical information regarding the conical intersection structure, allowing the exploration of the nonadiabatic dynamics from a completely different perspective.

EXPERIMENTAL SECTION

Experimental details have been described elsewhere.[16,37] Briefly, the 2-FTA sample was mixed with the neon carrier gas and expanded into vacuum through a nozzle orifice (ϕ = 100 μm) of the Even-Lavie pulsed valve at the repetition rate of 200 Hz with the backing pressure of ∼2 bar. The molecular beam was collimated by a skimmer (ϕ = 2 mm) and crossed by femtosecond ultraviolet laser pulses. The ions were accelerated in the time-of-flight tube toward a Chevron-type microchannel plate (MCP) detector coupled with the phosphor screen to be detected by the photomultiplier tube (PMT). The femtosecond pump (285 nm) and probe (300−330 nm) pulses (cross-correlation full width at half-maximum (FWHM) of 150 fs) were generated by two independent optical parametric amplifier (OPA) units (TOPAS-prime, Light Conversion). The OPA units were pumped by the 25:75 split of the fundamental output of 1 kHz femtosecond Ti:Sapphire regenerative amplifier system (Legend Elite-USP, Coherent, 35 fs) seeded by an 80 MHz femtosecond Ti:Sapphire oscillator (Vitara-T-HP, Coherent). The probe pulse was linearly polarized, which is parallel to the detection plane, and the polarization of the pump pulse was kept at the magic angle (54.7°). The pump−probe delay was manipulated by a 300 mm long linear translational stage (M-531.PD1, Physik Instrumente) combined with a retroreflector. The geometry optimization and excited-state calculations were carried out using the state-averaged complete active space self-consistent field (SA-CASSCF) method with the 6-311++G(2df,2pd) basis set using the Molpro program package.[75] For the lowest four electronic states of cationic 2-FTA, the (11,11) active space was generated using three pairs of π/π^* orbitals on the benzene ring, two pairs of σ/σ^* orbitals on the S-CH_3 bond, and a nonbonding p-type orbital of the sulfur atom. Potential energy curves along the S-CH_3 dihedral angle (φ) coordinate were obtained either by the geometry optimization of the D_0 state at each step of the φ increment (relaxed scan) or by freezing all of the geometric parameters other than φ (rigid scan). The single-state second-order perturbation theory (SS-

https://doi.org/10.1021/acs.jpca.1c04976
J. Phys. Chem. A XXXX, XXX, XXX−XXX

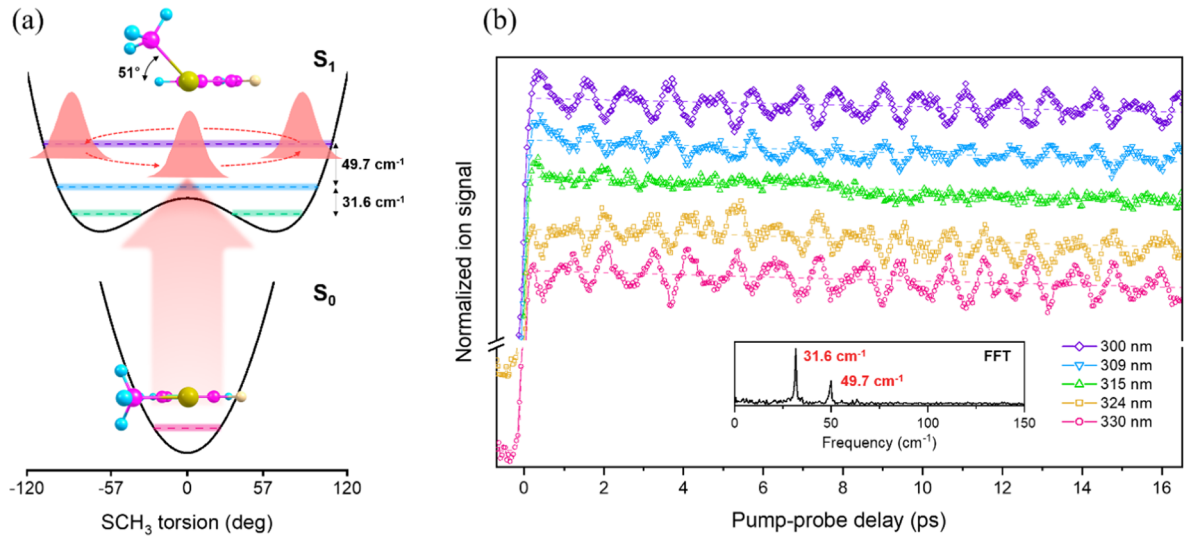

Figure 1. (a) Schematic potential energy curves of the S_0 and S_1 states along the S-CH_3 dihedral torsion angle (φ), where $\varphi = 0°$ indicates the S-CH_3 moiety faces the opposite direction of F atom at the same plane. The swing motion of the fs wavepacket is depicted. The S_1 geometry of 2-FTA at the ZPE level in our model potential is displayed on the top. (b) The parent ion transient of 2-FTA obtained at the pump wavelength of 285 nm and several probe wavelengths in the 330−300 nm range. In the inset, the fast Fourier transform (FFT) result obtained from the transient at λ_{probe} = 300 nm is shown.

CASPT2) correction was implemented with an imaginary level shift of 0.3 au.

RESULTS AND DISCUSSION

In our previous report, the resonance-enhanced two-photon ionization (R2PI) spectrum of 2-FTA obtained by the nanosecond laser pulse exhibits the prominent low-frequency S_1 vibronic progressions of 32 and 82 cm^{-1} corresponding to one (τ^1) and two quanta (τ^2) of SCH_3 torsion mode.[42] The equilibrium geometry and wavefunctions of the S_1 state of 2-FTA have been constructed by solving a Hamiltonian matrix in the discrete variable representation (DVR) with 1440 grid points of the SCH_3 torsion angle from −180 to 180° (Figure 1a).[76,77] The ground-state potential is modeled by a harmonic (quadratic) function, whereas the double-well potential energy function of $V(x) = 1/2kx^2 + Ae^{-Bx^2}$ has been employed for the depiction of S_1. Parameters of the model potentials are optimized to fit the experiment using the genetic algorithm (Supporting Information (SI)).[78] The resultant analytic S_1 potential energy curve suggests that the (most probable) dihedral angle of the S-CH_3 moiety should be 51° at the zero-point energy level. In other words, two minima of the potential energy curve are located at $\varphi = \pm 57°$ with a small barrier of 40 cm^{-1}. The out-of-plane dihedral angle in S_1 is found to be actually much nearer to the perpendicular geometry than the previously reported value of ∼12.5° predicted based on the unscaled *ab initio* calculations.[42] The Franck−Condon simulation based on the calculated wavefunctions of S_0 and S_1 then gives the band intensity ratio of $\tau^0:\tau^1:\tau^2$ = 1.0:1.8:0.4. This is in excellent agreement with the one-color R2PI experiment. The large negative anharmonicity (which is larger than unity for the steeper potential energy curve than predicted by the harmonic approximation) of $\gamma = [(\tau^2 - \tau^1)/(\tau^1 - \tau^0)]$ = 1.58 also strongly supports the largely distorted geometry of the S_1 2-FTA. This is quite consistent with the previous reports on other double-minima systems of 2-fluorophenol (γ = 1.28, $\varphi \approx 37°$),[67,79] 2-hydroxyphenol (γ = 1.23, $\varphi \approx 24°$),[68,80−82] or 2-methoxythiophenol (γ = 1.13, $\varphi \approx 20°$)[83,84] in terms of the correlation between γ and φ.[85]

The parent transients of 2-FTA obtained by the pump (285 nm) and probe (330−300 nm) laser pulses are shown in Figure 1b. Time-resolved quantum beats added on the slow decaying background ($\tau \approx$ 500 ps) are clearly observed. Fast Fourier transform (FFT) of the oscillatory part gives the beating frequencies of 31.6 and 49.7 cm^{-1}, and these exactly match with the frequency differences of coherently excited torsional modes of $(\tau^1 - \tau^0)$ and $(\tau^2 - \tau^1)$, respectively. The fs wavepacket interferogram thus confirms and refines the 2-FTA (S_1) structure of the nonplanar geometry with the precise dihedral angle of ∼51°. While the beating frequencies remain constant, the amplitudes and phases of the oscillatory part are found to be strongly modified by changing the probe laser wavelength. For instance, the phase in the transient obtained at λ_{probe} = 330 nm is completely inverted by the factor of π in the transient at λ_{probe} = 300 nm. Meanwhile, the oscillating amplitude almost vanishes in the transient at λ_{probe} = 315 nm. As a matter of fact, the decrease of the quantum beat amplitude could be attributed to the fact that the $D_0 \leftarrow S_1$ cross section becomes insensitive to the molecular planarity as the wider phase space of the cationic state (with respect to φ) is sampled with increasing the probe energy from 330 to 315 nm. And yet, it is quite remarkable that the beating amplitude gradually increases again as λ_{probe} decreases further with the inverted phase. This experimental finding indicates that there should be two distinct ionization processes having the totally different phases in the probing wavelength range of 330−300 nm. As the D_0 minimum-energy structure is planar,[55] the quantum beat is the consequence from the swing of the S_1 wavepacket along the out-of-plane dihedral angle. Namely, the planarity of the S_1 molecular structure is monitored by the $D_0 \leftarrow S_1$ cross section, which is either maximized or minimized as the S_1 wavepacket is located at the planar or nonplanar geometry, respectively. Since the temporal oscillation is solely due to the out-of-plane motion of the S_1 wavepacket, the ionization cross section is influenced only by the planarity of the cationic state.

https://doi.org/10.1021/acs.jpca.1c04976
J. Phys. Chem. A XXXX, XXX, XXX−XXX

Therefore, the experimental fact that the phase gets inverted as λ_{probe} changes from 330 to 300 nm indicates that the ionization cross section at λ_{probe} = 300 nm becomes maximized when the S_1 wavepacket is instantly located at the nonplanar geometry.

The adiabatic potential energy curves along φ have been calculated for the three lowest electronic states of the 2-FTA cation (Figure 2). The minimum-energy structure of D_0, optimized at the SA4-CASSCF(11,11)/6-311++G(2df,2pd) level, has been employed for the rigid or relaxed scan. All geometrical parameters of D_0 other than φ are kept frozen in the rigid scan, whereas those are continuously optimized in the relaxed scan. The PT2 correction has been made to obtain smoothly varying potential energy curves for all electronic states of D_2, D_1, and D_0. As mentioned above, the 2-FTA cation is planar at the global minimum of D_0, whereas it adopts the perpendicular geometry (φ = 90°) in both D_1 and D_2. The phase inversion in the quantum beat would have been nicely explained if the $D_1 \leftarrow S_1$ ionization could be invoked together with the $D_0 \leftarrow S_1$ transition as the former would show the completely inverted phase from the latter. However, from previous[55] and present experimental and theoretical results, the D_1 state is most likely located at least ~1 eV above the D_0 state, whereas the phase inversion has been found to occur at ~3000 cm^{-1} (0.37 eV) above the adiabatic ionization threshold (8.07 eV)[42] (Figure 1). Thus, it seems to be not appropriate to invoke the $D_1 \leftarrow S_1$ transition for the phase inversion observed in the current experiment. In this regard, it is quite notable that the D_0 state has a vertical minimum well at $\varphi \approx 135°$, while its global minimum adopts the planar geometry of φ = 0° along the potential energy curve calculated by the rigid scan. The nonplanar vertical minimum (which is the minimum along φ from the perspective of the $D_0 \leftarrow S_1$ vertical transition) is calculated to be ~0.4 eV above the planar global minimum. Although the much-lowered local minimum could be found at $\varphi \approx 180°$ in the relaxed scan, it should be emphasized that the S_1 wavepacket is subject to the prompt vertical transition in the ionization process. The vertical transition from S_1 then should experience the vertical minimum of D_0 at $\varphi \approx 135°$. Namely, the nonstationary S_1 wavepacket (pumped by 285 nm) is only allowed to be swung along the out-of-plane dihedral angle of φ, while all other geometrical parameters are frozen (see Figure S4 in the SI). Subsequent ionization by the fs probe laser pulse is strictly confined to the instant S_1 geometry given by the wavepacket location on the φ coordinate according to the Franck−Condon principle, validating that the rigid scanned potential energy curve should be employed for the explanation of the experiment. Based on the *ab initio* potential energy curves, the experiment has been simulated by calculating the vibrational wavefunction overlap between the nonstationary time-dependent S_1 wavepacket and the stationary D_0 state as a function of pump−probe time delay, Figure 3. The rigid scanned potential energy surface has been used to reflect stationary wavefunctions at the global (planar) and vertical ($\varphi \approx 135°$) minima. Most interestingly, the phase inversion could be perfectly reproduced by the simulation. And yet, the probe energy of ~6000 cm^{-1} above the adiabatic ionization threshold should be required for the observation of the clear phase inversion when *ab initio* potential energy curve is used without modification. This suggests that the D_0 vertical minimum energy might have been overestimated in the calculations. For the better match with the experiment, the model potential energy curve composed of two harmonic functions is employed with the variable energy gap (ΔE) between their distinct minima located at φ = 0° and $\Delta\varphi$. Two parameters are then varied until the simulation fits to the experiment to give ΔE = 2000 cm^{-1} and $\Delta\varphi$ = 135° (see Figure S5 in the SI).

Actually, this double-well D_0 potential energy curve may be helpful to resolve the previous disputed issue of the photoelectron spectroscopic results on thioanisole and 2-FTA regarding the possible existence of the conformational

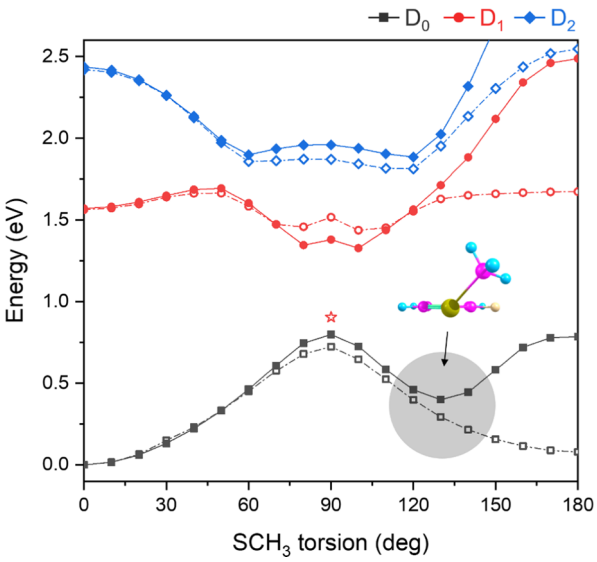

Figure 2. Calculated potential energy curves of 2-FTA in the ground and excited cationic states of D_0 (black), D_1 (red), or D_2 (blue) obtained at the level of SA4-CASSCF(11,11) with the single-state PT2 correction. All geometrical parameters except φ were frozen or optimized in the rigid (filled symbols connected with the solid line) or relaxed scan (opened symbols connected with the dotted line), respectively. The gray-shaded area represents the local minimum in the vertical transition (see the text). The minimum energy of the D_1 state optimized by itself at the same level of theory ($\varphi \approx 90°$) is denoted as a red star.

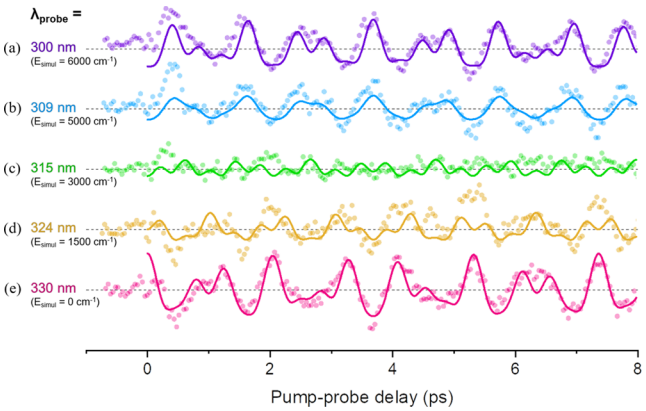

Figure 3. Simulations (solid lines) are overlaid with the experimental residuals after subtracting the exponential decay function of $\tau \approx 500$ ps (dots). Simulations are based on the rigid scanned potential energy curve of D_0 calculated at the SS-CASPT2 level. The probe laser wavelength used in the experiment is denoted for each transient, whereas the $D_0 \leftarrow S_1$ ionization energy (above the adiabatic ionization threshold) used in each simulation (E_{simul}) is shown within parentheses (see the text).

https://doi.org/10.1021/acs.jpca.1c04976
J. Phys. Chem. A XXXX, XXX, XXX−XXX

isomer of the perpendicular geometry in S_0. In the previously reported photoelectron spectrum of 2-FTA,[55] the broad $D_0 \leftarrow S_0$ band is accompanied with the significant shoulder in the high-binding-energy region. This shoulder could be now ascribed to the vertical minimum of D_0, which is accessed by the vertical transition. The growth of the shoulder intensity with increasing temperature had been previously reported in the photoelectron spectra of thioanisole.[45,48] This was attributed to the increase of the relative population of the perpendicular conformational isomer of thioanisole in S_0. And yet, it might be interpreted now to be due to the more excitation of the S_0 torsional modes at the higher temperature to give the more favorable Franck−Condon overlap to the vertical minimum of D_0 in the vertical ionization, which could be also applied to the case of 2-FTA in the same context. Amazingly, the binding energy associated with the shoulder in the photoelectron spectrum is approximately 0.3 eV higher than that of the main $D_0 \leftarrow S_0$ band, which is quite consistent with the gap of $\Delta E = 2000\ cm^{-1}$ (obtained by the simulation to the experiment) between the vertical and global minima of D_0.

CONCLUSIONS

In this work, the excited-state (S_1) molecular structure, in terms of the molecular planarity, has been precisely determined from the analysis of the fs wavepacket dynamics. Coherent excitation of the out-of-plane torsional progression bands (S_1) by the fs pump (285 nm) laser pulse prepares the nonstationary wavepacket, giving rise to the clear-cut quantum beat in the parent ion transient obtained by the pump−probe scheme. The beating frequencies are successfully reproduced by the S_1 double-well model potential, giving the nonplanar geometry of 2-FTA with the out-of-plane dihedral angle (φ) of 51° at the zero-point level. This nearly perpendicular molecular structure in S_1 should open the great opportunity to explore the otherwise blind unexplored aspect of the conical intersection dynamics. Intriguingly, the amplitudes and phases of the fs wavepacket interferogram are strongly modified as the ionization (probe) energy is changed. With the aid of *ab initio* calculations of the cationic states, it has been found that the 2-FTA cation (D_0) adopts the planar geometry at the global minimum, whereas it has a vertical minimum at $\varphi \approx 135°$ as the vertical ionization cross section is monitored along the dihedral angle and all of the other geometrical parameters except φ are frozen. The experiment is quite well reproduced by the simulation, especially when the double-well model potential curve is energetically modified (toward the lower location of the vertical minimum with respect to the global minimum in D_0) from *ab initio* values. The present experimental finding also shed new light on the long-disputed interpretation of the photoelectron spectroscopic results in the literature.

ASSOCIATED CONTENT

Supporting Information

The Supporting Information is available free of charge at https://pubs.acs.org/doi/10.1021/acs.jpca.1c04976.

Simulation details, full time-resolved ion yield data of 2-fluorothioanisole, spectra at different pump wavelengths, visual aid graphics for the theoretical interpretation, and quantum beat simulation using two harmonic potential functions (PDF)

AUTHOR INFORMATION

Corresponding Author

Sang Kyu Kim − *Department of Chemistry, KAIST, Daejeon 34141, Republic of Korea;* orcid.org/0000-0003-4803-1327; Email: sangkyukim@kaist.ac.kr

Authors

Junggil Kim − *Department of Chemistry, KAIST, Daejeon 34141, Republic of Korea*

Kyung Chul Woo − *Department of Chemistry, KAIST, Daejeon 34141, Republic of Korea;* Present Address: Division of Chemistry and Biological Chemistry, School of Physical and Mathematical Sciences, Nanyang Technological University, Singapore 637371, Singapore

Complete contact information is available at: https://pubs.acs.org/10.1021/acs.jpca.1c04976

Author Contributions

†J.K. and K.C.W. contributed equally to this work.

Notes

The authors declare no competing financial interest.

ACKNOWLEDGMENTS

This work was supported by National Research Foundation of Korea (NRF) under Project Numbers of 2018R1A2B3004534 and 2019K1A3A1A14064258.

REFERENCES

(1) Fischer, G. Chemical aspects of peptide bond isomerization. *Chem. Soc. Rev.* **2000**, *29*, 119−127.

(2) Schoenlein, R. W.; Peteanu, L. A.; Mathies, R. A.; Shank, C. V. The first step in vision: femtosecond isomerization of rhodopsin. *Science* **1991**, *254*, 412−415.

(3) Dian, B. C.; Longarte, A.; Zwier, T. S. Conformational dynamics in a dipeptide after single-mode vibrational excitation. *Science* **2002**, *296*, 2369−2373.

(4) Boyarkin, O. V. Cold ion spectroscopy for structural identifications of biomolecules. *Int. Rev. Phys. Chem.* **2018**, *37*, 559−606.

(5) Filsinger, F.; Erlekam, U.; von Helden, G.; Küpper, J.; Meijer, G. Selector for structural isomers of neutral molecules. *Phys. Rev. Lett.* **2008**, *100*, No. 133003.

(6) Chang, Y.-P.; Horke, D. A.; Trippel, S.; Küpper, J. Spatially-controlled complex molecules and their applications. *Int. Rev. Phys. Chem.* **2015**, *34*, 557−590.

(7) You, H. S.; Kim, J.; Han, S.; Ahn, D.-S.; Lim, J. S.; Kim, S. K. Spatial isolation of conformational isomers of hydroquinone and its water cluster using the Stark deflector. *J. Phys. Chem. A* **2018**, *122*, 1194−1199.

(8) Park, S. T.; Kim, S. K.; Kim, M. S. Observation of conformation-specific pathways in the photodissociation of 1-iodopropane ions. *Nature* **2002**, *415*, 306−308.

(9) Kim, M. H.; Shen, L.; Tao, H.; Martinez, T. J.; Suits, A. G. Conformationally controlled chemistry: excited-state dynamics dictate ground state reaction. *Science* **2007**, *315*, 1561−1565.

(10) Chang, Y.-P.; Długołęcki, K.; Küpper, J.; Rösch, D.; Wild, D.; Willitsch, S. Specific chemical reactivities of spatially separated 3-aminophenol conformers with cold Ca^+ ions. *Science* **2013**, *342*, 98−101.

(11) Lim, J. S.; Kim, S. K. Experimental probing of conical intersection dynamics in the photodissociation of thioanisole. *Nat. Chem.* **2010**, *2*, 627−632.

(12) Roberts, G. M.; Hadden, D. J.; Bergendahl, L. T.; Wenge, A. M.; Harris, S. J.; Karsili, T. N. V.; Ashfold, M. N. R.; Paterson, M. J.; Stavros, V. G. Exploring quantum phenomena and vibrational control in σ^* mediated photochemistry. *Chem. Sci.* **2013**, *4*, 993−1001.

(13) Han, S.; Lim, J. S.; Yoon, J.-H.; Lee, J.; Kim, S.-Y.; Kim, S. K. Conical intersection seam and bound resonances embedded in continuum observed in the photodissociation of thioanisole-d_3. *J. Chem. Phys.* **2014**, *140*, No. 054307.
(14) Kim, S.-Y.; Lee, J.; Kim, S. K. Conformer specific nonadiabatic reaction dynamics in photodissociation of partially deuterated thioanisoles. *Phys. Chem. Chem. Phys.* **2017**, *19*, 18902−18912.
(15) Li, S. L.; Truhlar, D. G. Full-dimensional mutli-state simulation of the photodissociation of thioanisole. *J. Chem. Phys.* **2017**, *147*, No. 044311.
(16) Woo, K. C.; Kang, D. H.; Kim, S. K. Real-time observation of nonadiabatic bifurcation dynamics at a conical intersection. *J. Am. Chem. Soc.* **2017**, *139*, 17152−17158.
(17) Lee, H.; Kim, S.-Y.; Kim, S. K. Multidimensional characterization of the conical intersection seam in the normal mode space. *Chem. Sci.* **2020**, *11*, 6856−6861.
(18) Devine, A. L.; Nix, M. G. D.; Dixon, R. N.; Ashfold, M. N. R. Near-ultraviolet photodissociation of thiophenol. *J. Phys. Chem. A* **2008**, *112*, 9563−9574.
(19) Ashfold, M. N. R.; Devine, A. L.; Dixon, R. N.; King, G. A.; Nix, M. G. D.; Oliver, T. A. A. Exploring nuclear motion through conical intersections in the UV photodissociation of phenols and thiophenol. *Proc. Natl. Acad. Sci. U.S.A.* **2008**, *105*, 12701−12706.
(20) Venkatesan, T. S.; Ramesh, S. G.; Lan, Z.; Domcke, W. Theoretical analysis of photoinduced H-atom elimination in thiophenol. *J. Chem. Phys.* **2012**, *136*, No. 174312.
(21) An, H.; Choi, H.; Lee, Y. S.; Baeck, K. K. Factors affecting the branching ratio of photodissociation: thiophenol studied through quantum wavepacket dynamics. *ChemPhysChem* **2015**, *16*, 1529−1534.
(22) You, H. S.; Han, S.; Lim, J. S.; Kim, S. K. ($\pi\pi^*/\pi\sigma^*$) conical intersection seam experimentally observed in the S-D bond dissociation reaction of thiophenol-d_1. *J. Phys. Chem. Lett.* **2015**, *6*, 3202−3208.
(23) Lin, G.-S.-M.; Xie, C.; Xie, D. Nonadiabatic effect in photodissociation dynamics of thiophenol via the $^1\pi\pi^*$ state. *J. Phys. Chem. A* **2018**, *122*, 5375−5382.
(24) Zhang, L.; Truhlar, D. G.; Sun, S. Full-dimensional three-state potential energy surfaces and state couplings for photodissociation of thiophenol. *J. Chem. Phys.* **2019**, *151*, No. 154306.
(25) Cho, D.; Rouxel, J. R.; Mukamel, S. Stimulated X-ray resonant Raman spectroscopy of conical intersections in thiophenol. *J. Phys. Chem. Lett.* **2020**, *11*, 4292−4297.
(26) Sobolewski, A. L.; Domcke, W.; Dedonder-Lardeux, C.; Jouvet, C. Excited-state hydrogen detachment and hydrogen transfer driven by repulsive $^1\pi\sigma^*$ states: a new paradigm for nonradiative decay in aromatic biomolecules. *Phys. Chem. Chem. Phys.* **2002**, *4*, 1093−1100.
(27) Tseng, C.-M.; Lee, Y. T.; Ni, C.-K. H atom elimination from the $\pi\sigma^*$ state in the photodissociation of phenol. *J. Chem. Phys.* **2004**, *121*, No. 2459.
(28) Lan, Z.; Domcke, W.; Vallet, V.; Sobolewski, A. L.; Mahapatra, S. Time-dependent quantum wave-packet description of the $^1\pi\sigma^*$ photochemistry of phenol. *J. Chem. Phys.* **2005**, *122*, No. 224315.
(29) Abe, M.; Ohtsuki, Y.; Fujimura, Y.; Lan, Z.; Domcke, W. Geometric phase effects in the coherent control of the branching ratio of photodissociation products of phenol. *J. Chem. Phys.* **2006**, *124*, No. 224316.
(30) Nix, M. G. D.; Devine, A. L.; Cronin, B.; Dixon, R. N.; Ashfold, M. N. R. High resolution photofragment translational spectroscopy studied of the near ultraviolet photolysis of phenol. *J. Chem. Phys.* **2006**, *125*, No. 133318.
(31) Nix, M. G. D.; Devine, A. L.; Dixon, R. N.; Ashfold, M. N. R. Observation of geometric phase effect induced photodisociation dynamics in phenol. *Chem. Phys. Lett.* **2008**, *463*, 305−308.
(32) Dixon, R. N.; Oliver, T. A. A.; Ashfold, M. N. R. Tunnelling under a conical intersection: application to the product vibrational state distributions in the UV photodissociation of phenols. *J. Chem. Phys.* **2011**, *134*, No. 194303.
(33) Roberts, G. M.; Chatterley, A. S.; Young, J. D.; Stavros, V. G. Direct observation of hydrogen tunneling dynamics in photoexcited phenol. *J. Phys. Chem. Lett.* **2012**, *3*, 348−352.
(34) Xu, X.; Zheng, J.; Yang, K. R.; Truhlar, D. G. Photodissociation dynamics of phenol: multistate trajectory simulations including tunneling. *J. Am. Chem. Soc.* **2014**, *136*, 16378−16386.
(35) Xie, C.; Ma, J.; Zhu, X.; Yarkony, D. R.; Xie, D.; Guo, H. Nonadiabatic tunneling in photodissociation of phenol. *J. Am. Chem. Soc.* **2016**, *138*, 7828−7831.
(36) Lai, H. Y.; Jhang, W. R.; Tseng, C.-M. Communication: mode-dependent excited-state lifetime of phenol under the S_1/S_2 conical intersection. *J. Chem. Phys.* **2018**, *149*, No. 031104.
(37) Woo, K. C.; Kim, S. K. Multidimensional H atom tunneling dynamics of phenol: interplay between vibrations and tunneling. *J. Phys. Chem. A* **2019**, *123*, 1529−1537.
(38) Woo, K. C.; Kim, S. K. Real-time tunneling dynamics through adiabatic potential energy surfaces shaped by a conical intersection. *J. Phys. Chem. Lett.* **2020**, *11*, 6730−6736.
(39) Woo, K. C.; Kim, J.; Kim, S. K. Conformer-specific tunneling dynamics dictated by the seam coordinate of the conical intersection. *J. Phys. Chem. Lett.* **2021**, *12*, 1854−1861.
(40) Crim, F. F. Vibrationally mediated photodissociation: exploring excited-state surfaces and controlling decomposition pathways. *Annu. Rev. Phys. Chem.* **1993**, *44*, 397−428.
(41) Bar, I.; Rosenwaks, S. Controlling bond cleavage and probing intramolecular dynamics via photodissociation of rovibrationally excited molecules. *Int. Rev. Phys. Chem.* **2001**, *20*, 711−749.
(42) Lim, J. S.; You, H. S.; Kim, S.-Y.; Kim, S. K. Experimental observation of nonadiabatic bifurcation dynamics at resonances in the continuum. *Chem. Sci.* **2019**, *10*, 2404−2412.
(43) Bock, H.; Wagner, G.; Kroner, J. Photoelectron spectra and molecular properties V. The perturbation of the benzene π system by methylthio substituents. *Tetrahedron Lett.* **1971**, *40*, 3713−3719.
(44) Dewar, P. S.; Ernstbrunner, E.; Gilmore, J. R.; Godfrey, M.; Mellor, J. M. Conformational analysis of alkyl aryl ethers and alkyl aryl sulphides by photoelectron spectroscopy. *Tetrahedron* **1974**, *30*, 2455−2459.
(45) Schweig, A.; Thon, N. Measurement of relative conformational stabilities by variable temperature photoelectron spectroscopy. A study of rotational isomerism in thioanisole. *Chem. Phys. Lett.* **1976**, *38*, 482−485.
(46) Zaripov, N. M. Electron diffraction study of the structure of the thioanisole molecule. *J. Struct. Chem.* **1977**, *17*, 640−642.
(47) Jones, I. W.; Tebby, J. C. Ultraviolet absorption spectra of alkyl benzyl sulphides. Conformational analysis of alkyl aryl sulphides. *J. Chem. Soc., Perkin Trans. 2* **1979**, 217−218.
(48) Honegger, E.; Heilbronner, E. The analysis of conformational equilibria by variable temperature photoelectron spectroscopy: a comment. *Chem. Phys. Lett.* **1981**, *81*, 615−619.
(49) Emsley, J. W.; Longeri, M.; Veracini, C. A.; Catalano, D.; Pedulli, G. F. The conformation of thioanisoles studied using nuclear magnetic resonance spectra of liquid crystalline solutions. *J. Chem. Soc., Perkin Trans. 2* **1982**, 1289−1296.
(50) Lumbroso, H.; Liégeois, Ch.; Testaferri, L.; Tiecco, M. Conformational preferences of poly(methylthio)benzenes. *J. Mol. Struct.* **1986**, *144*, 121−133.
(51) Schaefer, T.; Penner, G. H. Mechanisms of long-range ^{13}C, ^{13}C spin-spin coupling in thioanisole and its derivatives. Conformational applications. *Can. J. Chem.* **1988**, *66*, 1229−1238.
(52) Glass, R. S.; Broeker, J. L.; Jatcko, M. E. Distinguishing ionization from sulfur p-type lone pair orbitals and carbon π-molecular orbitals by He I/He II photoelectron spectroscopy. *Tetrahedron* **1989**, *45*, 1263−1272.
(53) Schaefer, T.; Sebastian, R.; Salman, S. R.; Baleja, J. D.; Penner, G. H.; McKinnon, D. M. The proximate coupling constant, $^5J(H,CH_3)$, and the torsional mobility of the thiomethyl group in some thioanisole derivatives. *Can. J. Chem.* **1991**, *69*, 620−624.
(54) Celebre, G.; Longeri, M.; Emsley, J. W. An NMR investigation using liquid crystalline solvents of the conformations of hindered

https://doi.org/10.1021/acs.jpca.1c04976
J. Phys. Chem. A XXXX, XXX, XXX−XXX

anisoles, thioanisole and selenoanisole. *Appl. Magn. Reson.* **1991**, *2*, 611−625.
(55) Chmielewski, D.; Werstiuk, N. H.; Wildman, T. A. Conformational preferences and barriers to internal rotation in fluorothioanisoles from long-range spin-spin couplings, photoelectron spectroscopy, and semiempirical molecular orbital calculations. *Can. J. Chem.* **1993**, *71*, 1741−1750.
(56) Bzhezovsky Vladimir, M.; Penkovsky, V. V.; Rozhenko, A. B.; Iksanova, S. V.; Kondratenko, N. V.; Yagupolsky, L. M. Multinuclear NMR spectroscopy and semi-empirical MNDO-PM3 quantum chemical investigations of the compounds C_6H_5XY (X = S, SO, SO_2; Y = CF_3, CH_3). *J. Fluorine Chem.* **1994**, *69*, 41−49.
(57) Vondrák, T.; Sato, S.; Špirko, V.; Kimura, K. Zero kinetic energy (ZEKE) photoelectron spectroscopic study of thioanisole and its van der Waals complexes with argon. *J. Phys. Chem. A* **1997**, *101*, 8631−8638.
(58) Dolgounitcheva, O.; Zakazewski, V. G.; Ortiz, J. V.; Ratovski, G. V. Electron propagator theory of conformational effects on anisole and thioanisole photoelectron spectra. *Int. J. Quantum Chem.* **1998**, *70*, 1037−1043.
(59) Colle, M. D.; Distefano, G.; Jones, D.; Modelli, A. Spectroscopic and theoretical determination of the electronic structure of anisole, thioanisole, and methoxy- and methylthiobenzonitriles: a contribution to the study of organic conducting polymers. *J. Phys. Chem. A* **2000**, *104*, 8227−8235.
(60) Bossa, M.; Morpurgo, S.; Stranges, S. The use of ab initio and DFT calculations in the interpretation of ultraviolet photoelectron spectra: the rotational isomerism of anisole and thioanisole as a case study. *J. Mol. Struct.: THEOCHEM* **2002**, *618*, 155−164.
(61) Gellini, C.; Moroni, L.; Muniz-Miranda, M. High overtones of the C-H stretching vibrations in anisole and thioanisole. *J. Phys. Chem. A* **2002**, *106*, 10999−11007.
(62) Yamakita, Y.; Isogai, Y.; Ohno, K. Large Raman-scattering activities for the low-frequency modes of substituted benzenes: induced polarizability and stereo-specific ring-substituted interactions. *J. Chem. Phys.* **2006**, *124*, No. 104301.
(63) Yamakita, Y.; Okazaki, T.; Ohno, K. Conformation-specific Raman bands and electronic conjugation in substituted thioanisoles. *J. Phys. Chem. A* **2008**, *112*, 12220−12227.
(64) Shishkov, I. F.; Khristenko, L. V.; Karasev, N. M.; Vilkov, L. V.; Oberhammer, H. Structure and conformation of thioanisole: gas electron diffraction and contradicting quantum chemical calculation. *J. Mol. Struct.* **2008**, *873*, 137−141.
(65) Nagasaka-Hoshino, M.; Isozaki, T.; Suzuki, T.; Ichimura, T.; Kawauchi, S. Molecular structure of jet-cooled thioanisole studied by laser-induced fluorescence spectroscopy and ab initio calculations: planar and/or perpendicular conformation? *Chem. Phys. Lett.* **2008**, *457*, 58−61.
(66) Hoshino-Nagasaka, M.; Suzuki, T.; Ichimura, T.; Kasahara, S.; Baba, M.; Kawauchi, S. Rotationally resolved high-resolution spectrum of the S_1-S_0 transition of jet-cooled thioanisole. *Phys. Chem. Chem. Phys.* **2010**, *12*, 13243−13247.
(67) Ling, F.; Li, S.; Song, X.; Wang, Y.; Long, J.; Zhang, B. Femtosecond time-resolved observation of butterfly vibration in electronically excited *o*-fluorophenol. *Sci. Rep.* **2017**, *7*, No. 15362.
(68) Young, J. D.; Staniforth, M.; Paterson, M. J.; Stavros, V. G. Torsional motion of the chromophore catechol following the absorption of ultraviolet light. *Phys. Rev. Lett.* **2015**, *114*, No. 233001.
(69) Young, J. D.; Staniforth, M.; Dean, J. C.; Roberts, G. M.; Mazzoni, F.; Karsili, T. N. V.; Ashfold, M. N. R.; Zwier, T. S.; Stavros, V. G. Towards understanding photodegradation pathways in lignins: the role of intramolecular hydrogen bonding in excited states. *J. Phys. Chem. Lett.* **2014**, *5*, 2138−2143.
(70) Hüter, O.; Sala, M.; Neumann, H.; Zhang, S.; Studzinski, H.; Egorova, D.; Temps, F. Long-lived coherence in pentafluorobenzene as a probe of $\pi\pi^*$-$\pi\sigma^*$ vibronic coupling. *J. Chem. Phys.* **2016**, *145*, No. 014302.
(71) Kus, J. A.; Hüter, O.; Temps, F. Real-time observation of multimode vibronic coherence in pentafluoropyridine. *J. Chem. Phys.* **2017**, *147*, No. 013938.
(72) Ling, F.; Li, S.; Song, X.; Tang, Y.; Wang, Y.; Zhang, B. Visualization of coherent nuclear motion between different geometries in photoexcited 2,4-difluorophenol. *Phys. Rev. A* **2017**, *95*, No. 043421.
(73) Ling, F.; Wang, Y.; Li, S.; Wei, J.; Tang, Y.; Zhang, B. Imaging reversible and irreversible structural evolution in photoexcited 2,4-difluoroaniline. *J. Phys. Chem. Lett.* **2018**, *9*, 5468−5473.
(74) Sala, M.; Egorova, D. Imaging large amplitude out-of-plane motion in photoexcited pentafluorobenzene using time-resolved photoelectron spectroscopy: a computational study. *Photochem. Photobiol. Sci.* **2018**, *17*, 1036.
(75) Werner, H.-J.; Knowles, P. J.; Knizia, G.; Manby, F. R.; Schütz, M. Molpro: a general-purpose quantum chemistry program package. *WIREs Comput. Mol. Sci.* **2012**, *2*, 242−253.
(76) Marston, C. C.; Balint-Kurti, G. G. The Fourier grid Hamiltonian method for bound state eigenvalues and eigenfunctions. *J. Chem. Phys.* **1989**, *91*, No. 3571.
(77) Luckhaus, D. 6D vibrational quantum dynamics: generalized coordinate discrete variable representation and (a)diabatic contraction. *J. Chem. Phys.* **2000**, *113*, No. 1329.
(78) Gulsen, M.; Smith, A. E.; Tate, D. M. A genetic algorithm approach to curve fitting. *Int. J. Prod. Res.* **1995**, *33*, 1911−1923.
(79) Remmers, K.; Meerts, W. L.; et al. Structural information on the S_0 and S_1 state of *o*-fluorophenol by hole burning and high resolution ultraviolet spectroscopy. *J. Chem. Phys.* **2000**, *112*, No. 6237.
(80) Gerhards, M.; Perl, W.; Schumm, S.; Henrichs, U.; Jacoby, C.; Kleinermanns, K. Structure and vibrations of catechol and catechol·$H_2O(D_2O)$ in the S_0 and S_1 state. *J. Chem. Phys.* **1996**, *104*, No. 9362.
(81) Gerhards, M.; Schumm, S.; Unterberg, C.; Kleinermanns, K. Structure and vibrations of catechol in the S_1 state and ionic ground state. *Chem. Phys. Lett.* **1998**, *294*, 65−70.
(82) King, G. A.; Oliver, T. A. A.; Dixon, R. N.; Ashfold, M. N. R. Vibrational energy redistribution in catechol during ultraviolet photolysis. *Phys. Chem. Chem. Phys.* **2012**, *14*, 3338−3345.
(83) Lim, J. S.; You, H. S.; Kim, S.-Y.; Kim, J.; Park, Y. C.; Kim, S. K. Vibronic structure and predissociation dynamics of 2-methoxythiophenol (S_1): the effect of intramolecular hydrogen bonding on nonadiabatic dynamics. *J. Chem. Phys.* **2019**, *151*, No. 244305.
(84) Lim, J. S. Spectroscopy and Photodissociation Dynamics on Nonplanar Excited State of Ortho-Substituted Thiophenol and Thioanisole. Ph.D. Thesis, Korea Advanced Instituted of Science and Technology: Daejeon, Korea, 2018.
(85) Dereka, B.; Yu, Q.; Lewis, N. H. C.; Carpenter, W. B.; Bowman, J. M.; Tokmakoff, A. Crossover from hydrogen to chemical bonding. *Science* **2021**, *371*, 160−164.

https://doi.org/10.1021/acs.jpca.1c04976
J. Phys. Chem. A XXXX, XXX, XXX−XXX